Title: Pangenomic analysis reveals plant NAD^+ manipulation as an important virulence activity of bacterial pathogen effectors

Michelle T. Hulin[1], Lionel Hill[2], Jonathan D. G. Jones[1], Wenbo Ma[1*]

[1] The Sainsbury Laboratory, Norwich Research Park, NR4 7UH, United Kingdom

[2] John Innes Centre, Norwich Research Park, NR4 7UH, United Kingdom

[*] Corresponding author: wenbo.ma@tsl.ac.uk

Author Contributions: W.M. and M.T.H. conceived the project. J.D.G.J contributed to experimental design. M.T.H. did the experiments and analyzed the data. L.H provided training and contributed to experimental design of LCMS. W.M., J.D.G.J and M.T.H. wrote the manuscript.

Competing Interest Statement: The authors declare no competing interests

Keywords: Pathogenicity, nucleosidase, plant immunity, TIR-NLR, cADPR variants, Type III secreted effectors, host-pathogen co-evolution

Abstract

Nicotinamide adenine dinucleotide (NAD^+) has emerged as a key component in prokaryotic and eukaryotic immune systems and the recent discovery that Toll/interleukin-1 receptor (TIR) proteins function as NAD^+ hydrolases (NADase) link NAD^+-derived small molecules with immune signalling. We investigated pathogen manipulation of host NAD^+ metabolism as a virulence strategy. Using the pangenome of the model bacterial pathogen *Pseudomonas syringae*, we conducted a structure-based similarity search from 35,000 orthogroups for type III effectors (T3Es) with potential NADase activity. Thirteen T3Es, including five newly identified candidates, were identified that possess domain(s) characteristic of seven NAD^+-hydrolyzing enzyme families. Most *P. syringae* strains that depend on the Type III secretion system to cause disease, encode at least one NAD^+-manipulating T3E, and many have several. We experimentally confirmed the type III-dependent secretion of a novel T3E, named HopBY, which shows structural similarity to both TIR and adenosine diphosphate ribose (ADPR) cyclase. Homologs of HopBY were predicted to be type VI effectors in diverse bacterial species, indicating potential recruitment of this activity by microbial proteins secreted during various interspecies interactions. HopBY efficiently hydrolyzes NAD^+ and specifically produces 2'cADPR, which can also be produced by TIR immune receptors of plants and other bacteria. Intriguingly, this

effector promoted bacterial virulence, indicating that 2'cADPR may not be the signalling molecule that directly initiates immunity. This study highlights a host-pathogen battle ground centred around NAD^+ metabolism and provides insight into the NAD^+-derived molecules involved in plant immunity.

Significance statement

NAD^+ metabolism plays a crucial role in plant and bacterial immunity. However, the diversity and scope of NAD^+ processing steps in immune signalling remain unclear. Furthermore, whether pathogens can manipulate NAD^+ metabolism to promote virulence is unknown. By conducting a pangenomic screen of the plant pathogen *P. syringae*, we found 13 type III effectors that potentially possess NADase activities, indicating that NAD^+ manipulation is an important virulence mechanism. Further characterization of a newly identified effector HopBY showed that it produces a cyclic ADP-ribose isomer (2'cADPR) and promotes bacterial infection and symptom development. This study clarifies the role of 2'cADPR in immune signalling and provides an example of effectors as useful molecular probes to understand immunity.

Introduction

The metabolite and redox agent nicotinamide adenine dinucleotide (NAD^+) is a universal co-factor and redox carrier involved in diverse cellular processes (1). Recent research on the Toll/Interleukin-1 receptor (TIR) domain proteins has established a central role of NAD^+ in immune signalling across biological kingdoms (2-4). Upon activation, TIRs cleaves NAD^+ through a N-glycosidase activity to produce nicotinamide (NAM), ADP-ribose (ADPR) and cyclic ADPR (5). It has recently been shown that different TIRs produce distinct isomers of cADPR including 2'cADPR and 3'cADPR (6). These TIR NADase products are thought to activate immune signalling. Plant and bacterial TIRs can make some of the same cADPR isomers and plant TIRs can activate bacterial anti-viral immunity proteins *in vitro* (4). In addition to cADPR isomers, other immunity-related products of plant TIR NADase and ADP-ribosylation activities have recently been identified including pRib-AMP/ADP, ADPr-ATP and diADPR (7, 8). Therefore, NAD^+-dependent immune signalling pathways are present in plants and bacteria (4, 9).

70 In plants, the TIR domain is often associated with intracellular immune receptors that
71 also contain the nucleotide binding and leucine-rich repeat (NLR) domains (10). NLR
72 proteins detect pathogen effectors that have entered plant cells and can promote
73 disease. Once activated, TIR-NLR immune receptors trigger immunity through the
74 downstream Enhanced Disease Susceptibility 1 (EDS1)-helper NLR pathways (11).
75 Activated TIR domains have been shown to hydrolyse NAD^+ and produce various
76 products, including the cADPR isomer 2'cADPR (3, 6-8, 12). TIR-produced molecules
77 pRib-AMP/ADP, ADPr-ATP and diADPR have been shown to bind to and activate
78 specific EDS1-helper NLR complexes (7, 8), potentially linking NADase activity of
79 activated TIR proteins to EDS1-dependent immune signalling. In addition, a TIR-only
80 resistance protein in plants, RBA1, exhibits 2',3'-cNMP synthase activity *in vitro* and
81 these cyclic nucleotides may also contribute to immunity (13).
82
83 Since NAD^+ metabolism contributes to innate immunity, we hypothesized that
84 manipulation of this process by pathogens might promote virulence. Pathogens rely
85 on effector proteins to manipulate host cellular processes, and effectors with NADase
86 activities have been reported. The bacterial animal pathogen *Brucella abortus*
87 produces TIR effectors BtpA and BtpB, which promote infection by reducing NAD^+
88 levels in the animal host and BtpA has also been shown to produce 2'cADPR (5, 14).
89 The plant pathogen *Pseudomonas syringae* produces a type III effector (T3E)
90 HopAM1 that also has a TIR domain. HopAM1 cleaves NAD^+ and produces 3'cADPR,
91 which was proposed to be responsible for the immune suppression activities of
92 HopAM1 during infection (6, 15). In addition, the bacteriophage protein Tad1
93 sequesters the TIR-produced molecule 2'cADPR and likely also 3'cADPR to overcome
94 anti-viral defence of the bacterial host (6, 9, 16). In addition to producing small
95 molecules from NAD^+ cleavage that might interfere with host signalling pathways, the
96 NAD^+ reduction activities of these effectors may directly contribute to host cell death
97 (14).
98
99 Enzymatic cleavage of NAD^+ can occur at either the pyrophosphate bond or the N-
100 glycosidic bond (Fig 1A). Pyrophosphate bonds can be cleaved by NUDIX
101 (nucleoside diphosphate linked to a variable moiety X) pyrophosphatases (17) and
102 phosphodiesterases (PDEs). The effector Avr3b produced by the oomycete pathogen
103 *Phytophthora sojae* harbors a NUDIX domain and can hydrolyse NADH, ADPR and

104 2',3'-cNMPs (13, 18). Enzymes that can cleave the N-glycosidic bond, apart from the
105 TIR proteins, include ADP-ribosyltransferases (ART), nucleoside hydrolases (NH),
106 ADPR cyclases, and sirtuins (Fig 1A). ARTs cleave NAD^+ to release ADPR, which is
107 often used for post-translational modifications of proteins and nucleic acids (19, 20).
108 ART effectors have been identified in various pathogens although most of them are
109 presumed to modify host protein targets (21). However, some ARTs act primarily as
110 NAD^+ glycohydrolases and don't require a protein substrate (22). Conceivably, at least
111 some ART effectors may function to manipulate NAD^+ metabolism. The *P. syringae*
112 T3E HopQ1 and the related *Xanthomonas euvesicatoria* T3E XopQ1 are nucleoside
113 hydrolases. HopQ1 was shown to alter purine metabolism (23) and activate cytokinin
114 signalling (23, 24). XopQ1 was also recently shown to hydrolyse 2',3'-cAMP (13). So
115 far, pathogen effectors with sirtuin or ADPR cyclase domains have not been identified.
116
117 Here, we employ pangenomic and structure-based similarity searches to identify
118 effectors with potential NADase activity from the species complex of the model
119 bacterial pathogen *P. syringae*. *P. syringae* relies on T3S to delivery effectors into
120 plant cells that suppress immunity and promote disease symptoms. We found *P.*
121 *syringae* encodes T3Es with six of the seven enzymatic activities that can hydrolyze
122 NAD^+, suggesting that manipulation of NAD^+ metabolism is an important virulence
123 mechanism. We then focused on a novel T3E, named HopBY, that possesses an
124 ADPR cyclase activity and characterized its potential virulence function. Intriguingly,
125 HopBY hydrolyzes NAD^+ and produces 2'cADPR *in vitro* and during infection.
126 2'cADPR can also be produced by plant TIR-NLRs, but our results indicate that it is
127 unlikely to be an activator of immune signalling.
128
129 **Results**
130 **Identification of NADases from the *P. syringae* pangenome**
131 The *P. syringae* species complex has been divided into phylogroups, which broadly
132 correspond to phylogenetic "species" sharing 95% Average Nucleotide Identity (ANI)
133 (25). Plant pathogens mainly belong to the monophyletic clade of "primary"
134 phylogroups and rely on a canonical Hrp1 type III secretion system (T3S) to cause
135 disease (26). The "secondary" phylogroups include environment-associated strains
136 which may not possess the Hrp1 T3S and encode very few T3Es when they do (27,
137 28).To examine NADase-encoding proteins across the species complex, 531 *P.*

138 *syringae* genomes were analysed. A phylogeny based on the core genome grouped
139 the strains into ≥ 95% identical ANI groups which loosely correspond to previously
140 defined phylogroups (Fig S1). Orthology analysis assigned the pangenome of
141 2,867,287 protein-encoding genes into 23,583 orthogroups (OGs), with an additional
142 11,608 singletons. In total, 35,191 OGs were further screened for candidate NADase
143 domains.
144
145 Two complementary approaches (HMMER and HHsearch) were employed to predict
146 proteins that may harbour any of the seven enzymatic domains related to NAD^+
147 hydrolysis (Pipeline illustrated in Fig S2A). These domains include ART, NUDIX, PDE,
148 TIR, sirtuin, ADPR cyclase, and nucleoside hydrolase (Fig 1A; Table S1). The
149 HMMER-based approach employed a Hidden Markov Model to identify any proteins
150 with sequence similarity to pfam seed alignments for each enzyme group. Using this
151 prediction method, 146 OGs were identified as candidate NADases. The HHsearch-
152 based approach used orthogroup sequence alignments with secondary structure
153 information. Based on HMM-HMM comparison with the PDB database, HHsearch
154 picked up 564 OGs as candidate NADases. Importantly, 136 of the 146 candidates
155 identified by HMMER were also identified by HHsearch (Table S2, full details in Table
156 S3), testifying the robustness of the structure-based prediction. When mapping on the
157 core genome phylogeny, the total of 574 candidate NADases are distributed across
158 the *P. syringae* species complex in both primary and secondary phylogroups without
159 a clear pattern in relation to pathogenesis (Fig S2B). This is consistent with their role
160 in regulating housekeeping processes and anti-viral immunity.
161
162 **Prediction of NADases as Type III effectors**
163 From the 574 candidate NADase OGs, we further identified T3Es because they are
164 major virulence factors in *P. syringae*. Our prediction pipeline included an initial screen
165 using the program EffectiveT3 (29) followed by a promoter search for the *hrp* box,
166 which is bound by the T3S-specific alternative sigma factor HrpL (30). The candidates
167 identified through this pipeline were further examined on their N-terminal amino acid
168 sequences for characteristics related to T3S-dependent secretion (31). The outcome
169 of this analysis revealed 13 NADase OGs as high confidence T3Es (Table 1; full list in
170 Table S4; Fig S3-S4). The robustness of this analysis is verified by the successful

171 identification of all the known T3Es with NADase-encoding domains including the ART
172 effectors HopF/HopBB, HopO1, AvrRpm, HopS, and HopU1, the NUDIX effector
173 HopAG1, the NH effector HopQ1, and the TIR effector HopAM1. The detection of
174 multiple non-overlapping homologies to different enzymes in the same protein also
175 revealed that HopAG1 carries a previously unknown ART domain on the N-terminus
176 in addition to the NUDIX domain on the C-terminus. Importantly, we identified five new
177 NADase T3E candidates, including two ARTs (OG5256, OG18195), one PDE
178 (OG4578), one TIR (OG8567), and one ADPR cyclase (OG18056).
179
180 The distribution of the 13 known NADase T3Es and new candidates was mapped on
181 the core genome phylogeny of *P. syringae* species complex (Fig 1B). A clear
182 difference between the primary and secondary phylogroups can be visualized, with
183 known and predicted NADase T3Es almost exclusively encoded by strains belonging
184 to the primary phylogroups, consistent with their potential role in host manipulation
185 (Fig 1B and Fig S5). 93% of the primary phylogroup strains have at least one NADase
186 T3Es and 72% possess T3Es belonging to more than one enzyme family. On average,
187 each primary phylogroup strain encodes three T3Es that potentially hydrolyze NAD^+.
188 NAD^+ hydrolysis is therefore a common virulence mechanism utilized by *P. syringae*
189 pathogens.
190
191 **OG18056 is a NADase with structural homology to both ADPR cyclases and**
192 **TIRs**
193 Considering the essential role of NAD-derived cADPR isomers in plant immunity, we
194 were particularly interested in a novel T3E candidate OG18056, which is predicted to
195 have an ADPR cyclase domain that has not been found in pathogen effectors. ADPR
196 cyclase shares a similar enzymatic activity with TIR and can also hydrolyze NAD^+ to
197 produce cADPR (32). Using AlphaFold2 (33), we generated a structural model for
198 OG18056. Superimposition of this model with the human ADPR cyclase CD38 showed
199 an RMSD value of 2.94 Å. The structural model of OG18056 also showed similarity
200 with the TIR domain of the human SARM1 protein with an RMSD value of 2.96 Å (Fig
201 2A). These results suggest that OG18056 possesses a fold that resembles both TIR
202 and ADPR cyclase, although our initial prediction only revealed similarity with ADPR
203 cyclase through HHsearch structure-based analysis.
204

205 The NAD^+ hydrolysis activity requires a catalytic glutamate (Glu, E) in TIR and ADPR
206 cyclase. Structural alignment revealed E305 in OG18056 to be located at the
207 corresponding position of the catalytic E642 in hSARM1 (2) as well as E226 in hCD38
208 (34) (Fig 2B). Furthermore, a ligand-binding pocket, containing the putative catalytic
209 residue E305, was predicted in OG18056 3D model using the program P2RANK with
210 a probability of 0.9 (35). Molecular docking revealed that NAD^+ could fit into this
211 predicted pocket with a binding affinity of -8.76 kcal/mol (Fig 2C). These results are
212 consistent with the hypothesis that OG18056 is an active NAD^+-cleaving enzyme.
213
214 To evaluate the enzymatic activity of OG18056, we used HPLC-MS analysis to detect
215 NAD^+ hydrolysis and production of various form(s) of cADPR. In a semi-*in vitro* assay
216 (36), 3xFLAG-tagged OG18056 and its predicted catalytic mutant $OG18056^{E305A}$ were
217 expressed in *Nicotiana benthamiana* by *Agrobacterium*-mediated transient
218 expression. Wild type and mutant OG18056 proteins were immunoprecipitated and
219 incubated with NAD^+. The resulting metabolites were extracted and analyzed by
220 LCMS. The results show that OG18056 produced a peak for m/z of 542.06, which is
221 consistent with that of cADPR, at a retention time of ~3.0 minutes (Fig 2D).
222 $OG18056^{E305A}$ did not produce this compound. The proteins were confirmed to be
223 expressed and immunoprecipitated (Fig 2E). These results demonstrate that
224 OG18056 is indeed an active NADase that produces a mass corresponding to cADPR.
225
226 **OG18056 (HopBY) produces 2'cADPR during bacterial infection**
227 To assess whether OG18056 is a secreted protein dependent on T3S, we tested its
228 expression pattern and T3S-dependent secretion using a minimal medium (Fig 3A).
229 The gene encoding OG18056, tagged at the C-terminus with a HA epitope, was
230 introduced into *P. syringae* pv. tomato strain DC3000 (PstDC3000) under its native
231 promoter. Bacterial cells were induced in a *hrp*-minimal medium (HM) and OG18056
232 proteins were detected in the cell culture supernatant by western blotting. We
233 observed that OG18056 had a minimal expression in the rich medium KB, but was
234 drastically induced in the HM medium, an expression pattern commonly observed in
235 T3S-related genes. Consistent with the detection of a *hrp* box in the promoter of
236 OG18056 gene, this result shows that OG18056 is regulated by T3S. Furthermore,
237 OG18056 proteins were detected in the supernatant of PstDC3000 cell culture, but not
238 in the supernatant of the Δ*hrcC* mutant of PstDC3000, which does not form a functional

239 T3S injectosome. These results suggest that OG18056 is likely a T3E that can be
240 secreted in a T3S-dependent manner. We therefore name this new T3E HopBY based
241 on the *P. syringae* T3E nomenclature system (28, 37).
242
243 We next examined whether HopBY hydrolyzes NAD^+ and produces isomer(s) of
244 cADPR during natural infection. HopBY or $HopBY^{E305A}$ was expressed in the D36E
245 mutant of PstDC3000 under its native promoter (Fig S6). D36E has the intact T3S but
246 lacks all 36 known T3Es, and is not pathogenic (38). The transformed bacteria were
247 then used to inoculate *Arabidopsis thaliana.* Eighteen hours post-infiltration,
248 metabolites were extracted from the inoculated leaf tissues and subjected to LCMS
249 analysis. We detected a clear peak corresponding to m/z 542.06 at the same retention
250 time (~3 min) as in the semi-*in vitro* assay (Fig 3B). This peak was absent in leaves
251 inoculated with D36E carrying the empty vector or expressing the catalytic mutant
252 $HopBY^{E305A}$, indicating that it is the product of HopBY NADase activity. As a control,
253 leaves inoculated with D36E expressing HopAM1 showed a peak with a retention time
254 of ~4.5 minutes, corresponding to 3'cADPR, as previously reported (6, 15). To
255 determine which isomer of cADPR was produced by HopBY, we ran LCMS on a cell
256 lysate of *E. coli* expressing AbTIR, which is produced by the opportunistic bacterial
257 pathogen *Acinetobacter baumannii*. AbTIR is known to produce 2'cADPR (6).
258 Interestingly, the HopBY product had the same retention time as the AbTIR product
259 (Fig 3C). When running a mixture of the different cADPR samples, a single peak with
260 m/z of 542.06 and a retention time of ~3.0 minutes appeared, suggesting that the
261 NAD^+ hydrolysis product of HopBY is likely the same or very similar to AbTIR, i.e.
262 2'cADPR (Fig 3D). Comparison of MS2 fragmentation profiles demonstrated that the
263 peak produced by HopBY generated similar fragment ions to the cADPR standard and
264 cADPR variants produced by other NADases, confirming that the HopBY product was
265 indeed a cADPR (Fig S7).
266
267 To determine if HopBY has any impact on overall NAD^+ levels during infection, we
268 measured the abundance of NAD^+ at days 0 and day 3 after inoculation with D36E
269 carrying either HopBY or HopAM1 (5×10^6 CFU/mL). NAD^+ levels showed a small but
270 significant reduction in leaf tissues inoculated with HopBY-expressing bacterium at
271 day 3 compared to day 0 (Fig. S8). This reduction was not observed in tissues

272 inoculated with D36E expressing HopAM1 or carrying the empty vector. These results
273 suggest that HopBY may reduce NAD^+ levels in host cells as a virulence mechanism.
274
275 **HopBY promotes bacterial infection and necrosis**
276 We next examined the potential virulence activity of HopBY during bacterial infection.
277 D36E expressing HopBY or the catalytic mutant $HopBY^{E305A}$ was used to inoculate *A.*
278 *thaliana* plants at a dose of 5 x 10^6 CFU/mL. We observed chlorotic symptoms in
279 leaves inoculated with D36E expressing HopBY, but not $HopBY^{E305A}$, after three days
280 (Fig 4A). When inoculated at a higher dose (1 x 10^8 CFU/mL), tissue collapse
281 appeared at 24 hours post inoculation, which is similar in appearance to immunity-
282 related hypersensitive response triggered by effectors recognized by NLRs, such as
283 AvrRps4 (Fig 4B). It is noteworthy that D36E expressing AvrRps4 did not induce the
284 chlorosis at the lower inoculum as HopBY did (Fig 4A). Similar to chlorosis, the cell
285 death-like phenotype was dependent on the NADase activity as the $HopBY^{E305A}$
286 mutant failed to induce this symptom. In addition, inoculation of *Pst* DC3000Δ*hrcC*
287 expressing HopBY did not cause these symptoms, which is consistent with the
288 previous results suggesting that HopBY is likely translocated during bacterial infection
289 in a T3S-dependent manner (Fig. S9).
290
291 Because 2'cADPR can be produced by some plant TIR-NLRs, it is therefore a
292 possibility that HopBY may activate an immune response, which would lead to cell
293 death due to hypersensitive response. To examine this, we inoculated D36E
294 expressing HopBY1 in the *A. thaliana* mutant *eds1-2*, which is critical for TIR-NLR-
295 mediated immune signalling (39). The results show that HopBY was still able to induce
296 the chlorosis (Fig 4A) and cell death-like phenotypes in the *eds1* mutant (Fig 4B). In
297 contrast, the cell death induced by AvrRps4 as a hypersensitive response was
298 abolished in *eds1-2* (Fig 4B). To further confirm HopBY did not trigger immunity in *A.*
299 *thaliana*, we evaluated the *in planta* bacterial population at three days post inoculation.
300 While expression of AvrRps4 caused a decline in bacterial population, HopBY actually
301 promoted infection (Fig 4C). This virulence activity was not observed in the catalytic
302 mutant $HopBY^{E305A}$. These results demonstrate that HopBY enhances bacterial
303 infection by promoting bacterial colonization and symptom development. These

304 virulence functions rely on its NADase activity, and possibly related to the production
305 of 2'cADPR.
306
307 **HopBY homologues are associated with T3 and T6 secretion systems**
308 HopBY is only present in three *P. syringae pv. coronafaciens* strains, which are
309 pathogens of grass species. The *hopBY* gene is flanked by transposase genes and
310 nearby genes encoding conjugation machinery (*virB* homologues). It is within 15 Kb
311 of T3E homologues *hopV1 and hopAA1* as well as a coronatine biosynthesis operon,
312 which also contributes to virulence (Fig S10A). This genomic location suggests that
313 *hopBY* may have been acquired via horizontal gene transfer. A skew in GC content
314 further indicates that this genomic region may represent a pathogenicity island (Fig
315 S10A).
316
317 Using BLASTP, we identified homologs of HopBY in diverse bacterial lineages ranging
318 in amino acid sequence identity from 26%-100%. HHsearch confirmed that these
319 homologs all have an ADPR cyclase-like fold on their C terminus (Table S5).
320 Examination of the genomic region surrounding all homologs revealed they are often
321 associated with transposons, indicating a strong signature of horizontal gene transfer
322 (Fig S10B). A phylogeny based on structure-guided protein sequence alignment
323 grouped these HopBY homologs into two clades (Fig 5A). The HopBY from *P. syringae*
324 is grouped with homologs from other *Pseudomonas* spp. as well as plant pathogenic
325 Enterobacteriaceae species within the genera *Brenneria* and *Pectobacterium*. All
326 these genomes contain genes encoding a Hrp1 T3S, the canonical T3S found in *P.*
327 *syringae*. Importantly, the homologous genes in this clade are all preceded by a *hrp*-
328 box promoter (Table S5), indicating that they are likely T3Es. In the *Brenneria* (n=2)
329 genomes, the *hopBY* homologous genes are present close to the T3S machinery gene
330 clusters, further supporting their identity as T3Es. The other clade includes more
331 distinct HopBY homologs including one in *Paraburkholderia* sp. ZP32-5, which was
332 also predicted as a possible T3E. *Paraburkholderia* sp. ZP32-5 contains the Hrp2 type
333 of T3S machinery and the HopBY homolog gene is located in close proximity to the
334 T3S gene cluster. Upstream of this gene there are PIP-box motifs, which are
335 associated with Hrp2 T3S-regulated gene expression. Therefore, this HopBY homolog
336 is likely also a T3E. Interestingly, other homologs in this clade are often located
337 adjacent to type VI secretion system (T6S) genes such as *vgrG*, *tssA*, *vasA* and *tssG*.

338 T6S is an important secretion system for bacterial interactions with other bacteria and
339 eukaryotes by delivering toxins that kill recipient cells (40). Indeed, these more distant
340 homologs of the *P. syringae* HopBY were predicted to be putative T6S effectors. Some
341 of these proteins have domains such as the N-terminal Rhs (Rearrangement Hotspot)
342 core domain, which are often found in T6Es (41).
343
344 Using structure models predicted by AlphaFold2 (Fig 5B), we aligned the predicted
345 ADPR cyclase domain in all the homologs to the *P. syringae* HopBY, which confirmed
346 their structural similarity with RMSD values ranging from 0 - 4.44 Å (Table S5). We
347 then aligned the region surrounding the catalytic residue E305 of *P. syringae* HopBY.
348 This revealed that the glutamate as well as an upstream tryptophan, which was shown
349 to be important for cyclization of the NAD^+ hydrolysis products (6, 32), are highly
350 conserved in all homologs, indicating they may be active enzymes (Fig 5C). The
351 existence of HopBY ADPR cyclase domain homologs across effectors from T3 and T6
352 secretion systems indicates this enzymatic activity may have been adopted by distinct
353 secretion systems that function in interspecies interactions.
354
355 **Discussion**
356 Exploiting the pangenomic diversity and the extensive genome sequence resources
357 of *P. syringae*, we conducted a comprehensive search to identify T3Es with enzymatic
358 activities that can hydrolyse NAD^+. This revealed host NAD^+ manipulation as a
359 virulence strategy in a model plant pathogen. *P. syringae* encodes a diverse set of
360 T3Es with six different enzymatic activities, which potentially modulate NAD^+
361 metabolism in plant cells during infection. Thus, manipulation of NAD^+ and NAD^+-
362 related molecules is an important virulence mechanism commonly used by diverse *P.*
363 *syringae* strains and likely by other plant and animal pathogens as well as
364 bacteriophages.
365
366 NAD^+ is a key metabolite that is involved in a wide range of cellular processes. NAD^+
367 depletion could lead to cell death (4). Therefore, it is possible that effectors contribute
368 to tissue damage through NAD^+ depletion, which may be related to the development
369 of disease symptoms. Indeed, the new T3E HopBY identified in this study caused
370 chlorosis and tissue collapse. HopBY delivery by D36E led to a moderate, but
371 statistically significant reduction in NAD^+ abundance in infected tissue (Fig S8). Since

372 not all plant cells in the leaf will receive effector delivery during infection, the observed
373 reduction in overall NAD^+ level may indicate significant depletion in those cells that do
374 receive HopBY. Conceivably, HopBY-associated necrotic symptoms is due to NAD^+
375 depletion in these cells. HopBY-associated phenotypes are EDS1-independent,
376 indicating that they are not due to activation of EDS1-mediated plant immunity but may
377 be a result of NAD^+ depletion. Overexpression of the TIR domain of AbTIR and some
378 plant TIRs in *N. benthamiana* also cause cell death independent of EDS1 (9, 42). This
379 suggests alternative immune signalling pathways may exist, or that these TIR proteins
380 may cause NAD^+ depletion when accumulated to a high level.
381
382 In addition to the potential impact of NAD^+ consumption activities, NADase effectors
383 could also promote disease through the production of specific metabolites. The newly
384 emerged role of NAD-derived small molecules in immune signalling leads to a
385 possibility in which pathogens can use NADase effectors to suppress immunity. We
386 can speculate that pathogen effectors could compete with host immune proteins for
387 substrates (43). In addition to NAD^+, the enzymatic domains identified from the *P.*
388 *syringae* T3Es may also use other molecules such as ADPR and cADPR as
389 substrates. Therefore, hydrolysis and depletion of immune signal molecules or their
390 precursors could be a virulence mechanism. Although these hypotheses remain to be
391 tested, investigation of the enzymatic activity of NADase effectors will offer a unique
392 opportunity to dissect immune signalling through NAD-derived small molecules.
393
394 TIR proteins across biological kingdoms generate cyclic nucleotide products that play
395 vital roles in immune signalling (3, 4). *P. syringae* produces HopAM1 as a TIR effector
396 and HopBY shows structural and functional similarity to both TIR and ADPR cyclase.
397 Both HopAM1 and HopBY could promote bacterial colonization indicating that they
398 could either suppress plant immunity (15) and/or promote an environment suitable for
399 disease progression. It is intriguing that plant and pathogen NADase activities can
400 result in opposite phenotypes (resistance vs susceptibility). An attractive possibility is
401 that these TIR/ADPR cyclase effectors produce distinct isomers that can activate
402 immune signalling. Indeed, HopAM1 produces 3'cADPR, distinct from the 2'cADPR
403 detected from the NAD^+ hydrolysis reaction of activated plant TIR proteins (3) and
404 could function as a negative regulator of plant immunity (6, 15). However, the
405 somewhat surprising finding that HopBY produced a significant amount of 2'cADPR

406 during bacterial infection reflects the complexity of NAD^+ metabolism in immune
407 response.
408
409 A role for 2'cADPR in TIR-NLR initiated immune signalling has been hypothesized but
410 not formally demonstrated (3). Several previous observations suggest that 2'cADPR
411 production alone is insufficient to activate immune signalling. A fusion receptor with
412 the bacterial AbTIR and a mammalian NLR did not activate cell death when expressed
413 in *N. benthamiana*, whilst several plant TIR-mammalian NLR fusions did (36).
414 Furthermore, expression of bacterial TIRs alone led to 2'cADPR production but did not
415 activate EDS1-mediated immunity in plants (4, 9). Finally, recent *in vitro* studies show
416 that EDS1-helper NLR complexes directly bind to pRib-AMP, pRib-ADP, ADPr-ATP
417 and diADPR. Therefore, although 2'cADPR can be produced by plant TIRs, it appears
418 insufficient to directly initiate EDS1-mediated immune signalling.
419
420 Homologous proteins to HopBY were identified across diverse bacterial lineages. The
421 *P. syringae* allele is closely related to other predicted T3Es from plant pathogens, but
422 the other homologs were predicted as T6Es, which are involved in bacteria-bacteria
423 and bacteria-eukaryotic interactions (40). NADase T6Es have been discovered before.
424 Two ART-like families of T6Es, Tse6 and Tne2, were involved in bacteria-bacteria
425 competition. Injecting into the recipient cells, Tse6 and Tne2 deplete NAD^+, leading to
426 cell death (45, 46). This mechanism is reminiscent to bacterial anti-viral immunity
427 which involves TIR signalling to activate the sirtuin ThsA to deplete NAD^+. It is
428 intriguing that HopBY homologs are widespread in bacteria as T6Es. Testing whether
429 these T6Es can function as cytotoxins in bacteria-bacteria or bacteria-eukaryote
430 competitions will be an interesting future experiment. Presumably, the bacterial strains
431 possessing T6 effectors related to HopBY must also encode an immunity protein or
432 mechanism to prevent the action of the T6 effector before secretion (46). Some of the
433 HopBY homologous T6Es contain the N-terminal Rhs domain (47). Rhs allows
434 diversification of T6Es at the C-terminal toxin domains via recombination (41). The
435 HopBY NADase domain likely recombined into these Rhs loci, generating a new
436 virulence function. Similarly, the HopBY homologous T3Es could also be created
437 through fusion to the T3S-dependent promoter and N-terminal secretion sequence via
438 the terminal reassortment mechanism (48). Therefore, the HopBY domain has been
439 incorporated into effectors for different interspecies competitions using distinct

440 secretion system machinery, demonstrating the importance of NAD^+ manipulation in
441 these antagonistic interactions.
442
443 Much remains to be discovered about the diverse NADase activities of TIR domains
444 and the complexity of their cyclic nucleotide products. The prevalence of pathogen
445 effectors with NADase activities testifies to the importance of NAD^+ metabolism as a
446 battleground in host-pathogen interactions. Understanding how effectors with NAD^+
447 hydrolysis activities promote virulence, and if and how they can disrupt immune
448 signalling pathways in plant hosts, will continue to provide new insights into immune
449 signalling and its circumvention in bacteria, animals, and plants.
450
451 **Methods**
452 Standard procedures used in this manuscript are documented in detail in the
453 Supplementary Methods. Specific methods developed here are included below.
454
455 **NADase T3E prediction**
456 The pipeline to identify nucleosidase candidates is presented in Fig S2A. For HMMER
457 (http://hmmer.org/) analysis, Pfam seed alignments for enzyme families (listed in Table
458 S1) were obtained from Pfam (http://pfam.xfam.org/) (downloaded on December 1st,
459 2020). The script hmmbuild was used to create a HMM profile for each seed alignment.
460 The command hmmsearch was used to screen all *P. syringae* proteins. HMMER
461 results were filtered based on a tolerant bit-score of $\geq$ 15 (49) and grouped by
462 orthogroup. Orthogroups with positive hits were further filtered to remove those in
463 which less than 5% of the orthogroup members were a hit as these rare hits may not
464 represent the orthogroup function.
465
466 HHsearch (50) was also used for each orthogroup to predict similarity to proteins in
467 the PDB database (downloaded on October 28th, 2021). First, a multi-sequence
468 alignment (MSA) was generated using ClustalW and a consensus sequence for each
469 orthogroup was generated using hhcon. Next, the secondary structure predicted by
470 PSIPRED was added to the alignment (51) before running HHsearch. Bash scripting
471 was used to extract candidates with hits towards NADase enzymes in the database

472 using a cutoff of ≥ 80% probability score. Two additional hits per protein with non-
473 overlapping regions were also identified.
474
475 Candidate orthogroups predicted with HMMER or HHsearch were next screened with
476 EffectiveT3 (29). Orthogroups containing hits with a score ≥ 0.9 were further analyzed
477 for putative *hrp* box sequences in their promoter region (within 1000 bp upstream of
478 the protein-coding sequence) using FIMO (30) based on the *hrp* box sequence
479 GGAACC(15-17N)CCACNNA as input.
480
481 Candidate T3Es were manually filtered based on the percentage of sequences within
482 the orthogroup predicted to be an effector (≥ 50%) and the percentage of these
483 sequences that contained a possible *hrp*-box promoter (≥ 25%). Orthogroups only
484 present in genomes without a predicted Hrp1 T3S were removed. Candidates T3Es
485 were then manually examined to determine if they had characteristic N-terminal
486 characteristics of *P. syringae* T3Es (31, 52). This included 1) a high percentage of
487 serines in the first 50 amino acids; 2) an aliphatic amino acid in positions 3 or 4; and
488 3) a lack of negatively charged residues within the first 12 positions. Genomic locations
489 of each T3E candidate gene were also manually examined using Geneious Prime
490 2022.0.1 to examine gene neighbourhoods (https://www.geneious.com).
491
492 **HPLC-MS**
493 Cyclic-ADP ribose was analysed using a 1290 Infinity UHPLC system equipped with
494 a 6546 Q-ToF (Agilent). Separation was on a 100×2.1mm 2.6µ Kinetex EVO C18
495 column connected in series to a 100×2.1mm 2.6µ Kintex F5 column (both
496 Phenomenex) using the following gradient of methanol (solvent B) versus 0.1% formic
497 acid adjusted to pH 6.0 with ammonium hydroxide (solvent A), run at 0.27 mL.min-1
498 and 35°C: 0 min, 0% B; 1.5 min, 3% B; 4.5 min, 15% B; 6.0 min, 60% B; 6.5 min, 95%
499 B; 7.5 min, 95% B; 7.6 min, 0% B; 11.6 min, 0% B. Detection was by positive
500 electrospray ionisation using the dual jet-stream ESI source. The instrument collected
501 full MS from m/z 100-1700 at 6 spectra per second, and automatic MS/MS of the two
502 most abundant precursors at 8 spectra per second, with an isolation width of m/z 4.0
503 ("medium") and 35% collision energy. Each precursor was ignored for 0.2 min, in
504 favour of less abundant precursors, after two MS/MS spectra had been collected.

505 Spray chamber conditions were 8 L.min-1 drying gas at 320°C, 35 psi nebulizer
506 pressure, 11 L.min-1 sheath gas at 350°C, 3500 Vcap, 1000V nozzle voltage, 175V
507 fragmentor, 65V skimmer, and 750V Octopole RF. The instrument was calibrated
508 according to the manufacturer's instructions before use, and reference masses
509 (121.0509; 922.0098) were used during the run to ensure mass accuracy.
510
511 **Acknowledgments:** We thank Dr. Alan Collmer for providing the *P. syringae* D36E
512 mutant and Ma lab members for discussions and technical support. We thank Dan
513 MacLean, Clara Jégousse and George Deeks for bioinformatic analysis support. Drs
514 He Zhao and Hee-Kyung Ahn provided AbTIR expressing *E. coli eds1-2 Arabidopsis*
515 seed and the pBBR1MCS-5::*avrRps4* plasmid. **Funding:** W.M. and J.J. are supported
516 by Gatsby Charitable Foundation and UKRI BBSRC Grant BBS/E/J/000PR9797.
517 **Competing Interests:** The authors declare no competing interests.
518
519 **Data and material availability:** All code are available at https://github.com/michhulin/
520 Pseudomonas. Materials are available from W.M. upon request under a materials
521 transfer agreement with the Sainsbury Laboratory.
522

523 **Table 1. Known NADase T3Es and predicted candidates in *P. syringae.***

Group	Ortho-group	No. genes	No. effectors	% effectors	No. *hrp* promoter	% *hrp* promoter	No. genomes	No. T3S+ genomes	% T3S+ genomes	Notes	Secretion signal score (out of 3)
ART	4303	339	332	98	299	90	188	187	99	HopF/BB	2
ART	5256	144	130	90	38	29	37	35	95	**Novel**	**3**
ART	5397	133	91	68	54	59	46	46	100	HopO1	3
ART	5686	112	103	92	91	88	87	87	100	AvrRpm	3
ART	6340	69	54	78	53	98	53	53	100	HopS	3
ART	9885	14	14	100	10	71	10	10	100	HopU1	3
ART	18195	3	3	100	3	100	3	3	100	**Novel**	**3**
ART[a]	4463	297	223	75	213	96	213	213	100	HopAG1	3
NH	4871	195	124	64	121	98	118	117	99	HopQ1	2
NUDIX	4463	297	223	75	213	96	213	213	100	HopAG1	3
PDE	4578	258	214	83	102	48	101	100	99	**Novel**	**2**
TIR	6638	55	49	89	45	92	38	37	97	HopAM1	3
TIR	8567	23	21	91	15	71	14	14	100	**Novel**	**2**
ADPR cyclase	18056	3	3	100	3	100	3	3	100	**Novel**	**3**

524
525 No. genes: number of genes in orthogroup.
526 No. effectors: number of genes within orthogroup that were predicted to encode an effector.
527 % effectors: % orthogroup that may encode effector.
528 No. *hrp* promoter: Number of predicted effector genes per orthogroup that had a predicted *hrp* box
529 % *hrp* promoter: % effector genes in orthogroup that had *hrp* promoter.
530 No. T3S+ genomes: Number of genomes encoding the genes in each orthogroup predicted as
531 effectors with a *hrp* box which have the genes required for Hrp1 T3S machinery.
532 % genomes with Hrp1 T3S: % of effector genes with a *hrp* box per orthogroup that were in genomes
533 encoding Hrp1 T3S.
534 Secretion signal score: A score from 0-3 based on three previously defined criteria of T3E secretion
535 signals:1) a high % serines; 2) a lack of negative amino acids in the first 12 residues; 3) an aliphatic
536 amino acid at position 3 or 4.
537 [a] Although the main hit of OG0004463 (HopAG1) was a NUDIX domain, a further domain with
538 homology to ART was predicted at a different region of the protein.
539
540
541
542
543
544
545
546
547
548
549
550

551 **Figure legends**

552 **Figure 1. Predicted NADases as type III effectors in *P. syringae* species complex.**

553 A) Enzymes that can cleave NAD^+. The NUDIX (nucleoside diphosphate linked to a
554 variable moiety X) enzymes and phosphodiesterases (PDEs) cleave the
555 pyrophosphate bond. ADP-ribosyltransferases (ART), nucleoside hydrolases
556 (NH), ADPR cyclases, and sirtuins cleave the N-glycosidic bond.

557 B) Predicted NADase type III effectors (T3Es) from the pangenome of *P. syringae*.
558 Eight known T3Es and five new candidates are mapped onto the maximum-
559 likelihood core genome phylogeny of *P. syringae* species complex. Strains in the
560 primary phylogroups are coloured in red in the phylogenetic tree. Ring 1-6 each
561 represents one of the six enzymatic families with NADase activity. Known T3Es
562 with ART domains are in the order (from inside to outside) of HopF/BB, HopO1,
563 AvrRpm, HopS, HopU1, HopAG1. Grey squares indicate the orthogroup of a
564 specific enzymatic domain is present in the strain but does not have a putative *hrp*
565 box in the promoter.

566

567 **Figure 2. OG18056 is an active NADase that produces a variant of cADPR.**

568 A) Alignment of a structural model of OG18056 (predicted by AlphaFold2, in cyan)
569 with a human ADPR cyclase CD38 (6VUA, in grey) and the TIR domain of human
570 SARM1 (6O0R, 561-700 aa, in light brown). For visualisation purposes, sequences
571 outside the alignment region were removed and those that did not align within the
572 region are more transparent. The position of the predicted catalytic Glu residues,
573 which are aligned in the three proteins, is highlighted with a box.

574 B) A close-up of alignments of OG18056 with TIR-hSARM1 (upper) and hCD38
575 (lower) at the predicted catalytic site showing a Glu E305 in OG18056 that is
576 aligned with the catalytic residues E642 in TIR-hSARM1 and E226 in hCD38.

577 C) Electrostatic image of the surface of the structure model of OG18056 with regions
578 of positive, neutral, and negative charge coloured in blue, white, and red
579 respectively. A molecule of NAD^+ was docked into the predicted catalytic pocket.

580 D) HPLC chromatograms showing the cADPR product produced by OG18056 using
581 a semi-*in vitro* assay. OG18056 and $OG18056^{E305A}$ were expressed in *N.*
582 *benthamiana*. After immuno-precipitation, the proteins were incubated with NAD^+
583 for one hour before subjected to LCMS analysis. The controls were NAD^+ only
584 without addition of beads and immunoprecipitation of proteins from leaves

585 infiltrated with *Agrobacterium* carrying an empty vector (EV). Peaks corresponding
586 to m/z 542.06 (cADPR) and m/z 664.11 (NAD^+) were identified.
587 E) Immunoblots detecting the expression of OG18056 and $OG18056^{E305A}$ in *N.*
588 *benthamiana* (input) and after immunoprecipitated (IP). The IPed samples were
589 used for the LCMS assays. OG18056 and $OG18056^{E305A}$ were tagged with C-
590 terminal 3xFLAG. Empty vector (EV) was included as a control. Ponceau Staining
591 (PS) of the membrane was used as a loading control.
592
593 **Figure 3: OG18056 (HopBY) is a true type III effector that produces 2'cADPR**
594 **during bacterial infection.**
595 A) Immunoblots showing the induction and secretion of OG18056 in a T3S-dependent
596 manner by *P. syringae*. OG18056-HA was introduced in PstDC3000 or the T3S
597 mutant Δ*hrcC* under its native promoter. The bacteria were cultured in the rich
598 medium King's B (KB) or a Hrp-inducing minimal medium (HM). Proteins were
599 extracted from cell pellet (cp) or supernatant (sn) and OG18056 was detected by
600 western blotting using an anti-HA antibody. Ponceau Staining (PS) of the
601 membrane was used as a loading control. OG18056 is hereafter referred to as
602 HopBY.
603 B) HPLC chromatograms of *A. thaliana* leaf extracts using tissues 18 hours post-
604 inoculation with the *P. syringae* "effectorless" mutant D36E expressing HopBY.
605 Leaves treated with 10mM $MgCl_2$ was used as the control. Leaves inoculated with
606 D36E carrying an empty vector (EV), or expressing $HopBY^{E305A}$, HopAM1 or
607 $HopAM1^{E191A}$ were included for comparison. All effectors were cloned under their
608 native promoter. Peaks corresponding to m/z 542.06 (cADPR) and m/z 664.11
609 (NAD^+) were identified.
610 C) HPLC chromatograms of different cADPR variants compared to the product of
611 HopBY (extracted from *A. thaliana* inoculated with D36E expressing HopBY).
612 2'cADPR was detected from cell lysate of *E. coli* expressing AbTIR, and 3'cADPR
613 was detected from *A. thaliana* leaves inoculated with D36E expressing HopAM1.
614 cADPR and NAD^+ were purchased from Sigma.
615 D) HPLC chromatogram of a mixture of samples as described in Panel C. Only one
616 peak appeared at a retention time 3.0 min, indicating that the HopBY product is
617 likely 2'cADPR. At: *Arabidopsis thaliana*; Ec: *E. coli*

618

619 **Figure 4: HopBY enhanced bacterial growth and triggered disease-like**
620 **symptoms in *A. thaliana*.**

621 A) Disease symptom development in *A. thaliana* inoculated by the *P. syringae* mutant
622 D36E carrying the empty vector (EV), or expressing HopBY, HopBY^{E305A} or
623 AvrRps4. Adult leaves of wildtype (WT) and *eds1-2* mutant were inoculated with
624 bacterial suspensions of 5 x 10^6 CFU/mL and symptoms were imaged at 3 days
625 post inoculation.

626 B) Cell death-like phenotype induced by HopBY at a high inoculum dose (5 x 10^8
627 CFU/mL) in an EDS1-independent manner. D36E expressing individual effectors
628 were used to inoculate *A. thaliana* adult leaves, which were imaged one day post
629 inoculation.

630 C) Bacterial populations (in Log CFU/cm^2) measured at 0 and 3 days post inoculation
631 in wildtype *A. thaliana*. D36E transformants were used to inoculate adult leaves at
632 5 x10^5 CFU/mL. Individual data points with different colors represent results from
633 three separate experiments. Tukey-HSD significance groups extracted from
634 ANOVA are presented ($p<0.05$). HopBY was cloned in the vector pUCP20tk but
635 AvrRps4 was cloned in the vector pBBR1MCS-5. Therefore both empty vectors
636 (pUCP EV and pBBR EV) were included as controls.

637

638 **Fig 5: HopBY homologs are present in diverse bacterial species as type III or**
639 **type VI effectors.**

640 A) Maximum-likelihood phylogeny of HopBY homologs using structure-guided protein
641 sequence alignment. The homologs are grouped in two clades with the *P. syringae*
642 HopBY labeled as "1". Tips are labelled as green (T3Es with a *hrp* box in the
643 promoter) or pink (putative T6Es). The predicted Hrp2 T3E was labelled as black.
644 The scale shows substitutions per site.

645 B) AlphaFold2 models of HopBY homologs, which show diverse overall structures.
646 Numbers correspond to panel A. 1: *P. syringae coronafaciens* ICMP 4457, 2:
647 *Brenneria* sp. EniD312, 3: *Gammaproteobacteria* RS470, 4: *Paraburkholderia* sp.
648 ZP32-5, 5: *Duganella* sp. CF517, 6: *Pseudomonas frederiksbergensis* PgKB32.
649 The HopBY-like ADPR cyclase domain is always on the C terminus of each protein,
650 which is highlighted in cyan.

651 **C)** Sequence logo showing the conservation of residues in the region surrounding the
652 catalytic Glu residue (corresponding to positions 300-310 aa in the *P. syringae*
653 HopBY). W301 and E305 are 100% conserved in all the 44 homologs.

654 **References**

655 1. P. Petriacq, J. Ton, O. Patrit, G. Tcherkez, B. Gakiere, NAD Acts as an Integral
656 Regulator of Multiple Defense Layers. *Plant Physiol* **172**, 1465-1479 (2016).
657 2. K. Essuman *et al.*, The SARM1 Toll/Interleukin-1 Receptor Domain Possesses
658 Intrinsic NAD(+) Cleavage Activity that Promotes Pathological Axonal Degeneration.
659 *Neuron* **93**, 1334-1343 e1335 (2017).
660 3. L. Wan *et al.*, TIR domains of plant immune receptors are NAD(+)-cleaving enzymes
661 that promote cell death. *Science* **365**, 799-803 (2019).
662 4. G. Ofir *et al.*, Antiviral activity of bacterial TIR domains via immune signalling
663 molecules. *Nature* **600**, 116-120 (2021).
664 5. K. Essuman *et al.*, TIR Domain Proteins Are an Ancient Family of NAD(+)-
665 Consuming Enzymes. *Curr Biol* **28**, 421-430 e424 (2018).
666 6. M. K. Manik *et al.*, Chemical structures of cyclic ADP ribose (cADPR) isomers and
667 the molecular basis of their production and signaling. *Science*
668 10.1126/science.adc8969 (2022).
669 7. S. Huang *et al.*, Identification and receptor mechanism of TIR-catalyzed small
670 molecules in plant immunity. *BioRxiv* 10.1101/2022.04.01.486681 (2022).
671 8. A. Jia *et al.*, TIR-catalyzed ADP-ribosylation reactions produce signaling molecules
672 for plant immunity. *BioRxiv* 10.1101/2022.05.02.490369 (2022).
673 9. A. M. Bayless *et al.*, Plant and prokaryotic TIR domains generate distinct cyclic
674 ADPR NADase products. *BioRxiv* 10.1101/2022.09.19.508568 (2022).
675 10. J. Kourelis, R. A. L. van der Hoorn, Defended to the Nines: 25 Years of Resistance
676 Gene Cloning Identifies Nine Mechanisms for R Protein Function. *Plant Cell* **30**, 285-
677 299 (2018).
678 11. N. Adlung *et al.*, Non-host Resistance Induced by the *Xanthomonas* Effector XopQ Is
679 Widespread within the Genus *Nicotiana* and Functionally Depends on EDS1. *Front*
680 *Plant Sci* **7**, 1796 (2016).
681 12. S. Ma *et al.*, NAD+ cleavage activity by animal and plant TIR domains in cell death
682 pathways. *Science* **370** (2020).
683 13. D. Yu *et al.*, TIR domains of plant immune receptors are 2',3'-cAMP/cGMP
684 synthetases mediating cell death. *Cell* 10.1016/j.cell.2022.04.032 (2022).
685 14. J. M. Coronas-Serna *et al.*, The TIR-domain containing effectors BtpA and BtpB from
686 *Brucella abortus* impact NAD metabolism. *PLoS Pathog* **16**, e1007979 (2020).
687 15. S. Eastman *et al.*, A phytobacterial TIR domain effector manipulates NAD(+) to
688 promote virulence. *New Phytol* **233**, 890-904 (2022).
689 16. A. Leavitt *et al.*, Viruses inhibit TIR gcADPR signaling to overcome bacterial
690 defense. *BioRxiv* 10.1101/2022.05.03.490397 (2022).
691 17. J. R. Srouji, A. Xu, A. Park, J. F. Kirsch, S. E. Brenner, The evolution of function
692 within the Nudix homology clan. *Proteins* **85**, 775-811 (2017).
693 18. S. Dong *et al.*, *Phytophthora sojae* avirulence effector Avr3b is a secreted NADH and
694 ADP-ribose pyrophosphorylase that modulates plant immunity. *PLoS Pathog* **7**,
695 e1002353 (2011).
696 19. D. Corda, M. Di Girolamo, Functional aspects of protein mono-ADP-ribosylation.
697 *The EMBO Journal* **22**, 1953–1958 (2003).
698 20. T. Takamura-Enya *et al.*, Mono(ADP-ribosyl)ation of 2'-deoxyguanosine residue in
699 DNA by an apoptosis-inducing protein, pierisin-1, from cabbage butterfly. *Proc Natl*
700 *Acad Sci U S A* **98**, 12414-12419 (2001).
701 21. K. J. Schreiber, I. J. Chau-Ly, J. D. Lewis, What the Wild Things Do: Mechanisms of
702 Plant Host Manipulation by Bacterial Type III-Secreted Effector Proteins.
703 *Microorganisms* **9** (2021).

22. J. Ghosh, M. G. Caparon, Specificity of *Streptococcus pyogenes* NAD(+) glycohydrolase in cytolysin-mediated translocation. *Mol Microbiol* **62**, 1203-1214 (2006).
23. W. Li, Y. H. Chiang, G. Coaker, The HopQ1 effector's nucleoside hydrolase-like domain is required for bacterial virulence in arabidopsis and tomato, but not host recognition in tobacco. *PLoS One* **8**, e59684 (2013).
24. D. R. Hann *et al.*, The *Pseudomonas* type III effector HopQ1 activates cytokinin signaling and interferes with plant innate immunity. *New Phytol* **201**, 585-598 (2014).
25. M. Gomila, A. Busquets, M. Mulet, E. Garcia-Valdes, J. Lalucat, Clarification of Taxonomic Status within the *Pseudomonas syringae* Species Group Based on a Phylogenomic Analysis. *Front Microbiol* **8**, 2422 (2017).
26. G. R. Cornelis, The type III secretion injectisome. *Nat Rev Microbiol* **4**, 811-825 (2006).
27. X. F. Xin, B. Kvitko, S. Y. He, *Pseudomonas syringae:* what it takes to be a pathogen. *Nat Rev Microbiol* **16**, 316-328 (2018).
28. M. M. Dillon *et al.*, Recombination of ecologically and evolutionarily significant loci maintains genetic cohesion in the *Pseudomonas syringae* species complex. *Genome Biol* **20**, 3 (2019).
29. V. Eichinger *et al.*, EffectiveDB--updates and novel features for a better annotation of bacterial secreted proteins and Type III, IV, VI secretion systems. *Nucleic Acids Res* **44**, D669-674 (2016).
30. C. E. Grant, T. L. Bailey, W. S. Noble, FIMO: scanning for occurrences of a given motif. *Bioinformatics* **27**, 1017-1018 (2011).
31. D. Guttman *et al.*, A Functional Screen for the Type III (Hrp) Secretome of the Plant Pathogen Pseudomonas syringae. *Science* **295**, 1722-1726 (2002).
32. R. Graeff *et al.*, Mechanism of cyclizing NAD to cyclic ADP-ribose by ADP-ribosyl cyclase and CD38. *J Biol Chem* **284**, 27629-27636 (2009).
33. M. Mirdita *et al.*, ColabFold - Making protein folding accessible to all. *BioRxiv* 10.1101/2021.08.15.456425 (2022).
34. C. Munshi *et al.*, Identification of the enzymatic active site of CD38 by site-directed mutagenesis. *J Biol Chem* **275**, 21566-21571 (2000).
35. R. Krivak, D. Hoksza, P2Rank: machine learning based tool for rapid and accurate prediction of ligand binding sites from protein structure. *J Cheminform* **10**, 39 (2018).
36. Z. Duxbury *et al.*, Induced proximity of a TIR signaling domain on a plant-mammalian NLR chimera activates defense in plants. *Proc Natl Acad Sci U S A* **117**, 18832-18839 (2020).
37. M. Lindeberg *et al.*, Proposed Guidelines for a Unified Nomenclature and Phylogenetic Analysis of Type III Hop Effector Proteins in the Plant Pathogen Pseudomonas syringae. *Mol Plant Microbe Interact* **18**, 275-282 (2005).
38. H. L. Wei *et al.*, *Pseudomonas syringae* pv. *tomato* DC3000 Type III Secretion Effector Polymutants Reveal an Interplay between HopAD1 and AvrPtoB. *Cell Host Microbe* **17**, 752-762 (2015).
39. A. Falk *et al.*, EDS1, an essential component of R gene-mediated disease resistance in Arabidopsis has homology to eukaryotic lipases. *Proc Natl Acad Sci U S A* **96**, 3292-3297 (1999).
40. J. Monjaras Feria, M. A. Valvano, An Overview of Anti-Eukaryotic T6SS Effectors. *Front Cell Infect Microbiol* **10**, 584751 (2020).
41. S. J. Poole *et al.*, Identification of functional toxin/immunity genes linked to contact-dependent growth inhibition (CDI) and rearrangement hotspot (Rhs) systems. *PLoS Genet* **7**, e1002217 (2011).

754 42. O. Johanndrees *et al.*, Differential EDS1 requirement for cell death activities of plant
755 TIR-domain proteins. *BioRxiv* 10.1101/2021.11.29.470438 (2021).
756 43. K. Essuman, J. Milbrandt, J. L. Dangl, M. T. Nishimura, Shared TIR enzymatic
757 functions regulate cell death and immunity across the tree of life. *Science* **377**,
758 eabo0001 (2022).
759 44. J. Steinbeck *et al.*, In Vivo NADH/NAD(+) Biosensing Reveals the Dynamics of
760 Cytosolic Redox Metabolism in Plants. *Plant Cell* **32**, 3324-3345 (2020).
761 45. J. C. Whitney *et al.*, An interbacterial NAD(P)(+) glycohydrolase toxin requires
762 elongation factor Tu for delivery to target cells. *Cell* **163**, 607-619 (2015).
763 46. J. Y. Tang, N. P. Bullen, S. Ahmad, J. C. Whitney, Diverse NADase effector families
764 mediate interbacterial antagonism via the type VI secretion system. *J Biol Chem* **293**,
765 1504-1514 (2018).
766 47. D. Jurenas *et al.*, Mounting, structure and autocleavage of a type VI secretion-
767 associated Rhs polymorphic toxin. *Nat Commun* **12**, 6998 (2021).
768 48. J. Stavrinides, W. Ma, D. S. Guttman, Terminal reassortment drives the quantum
769 evolution of type III effectors in bacterial pathogens. *PLoS Pathog* **2**, e104 (2006).
770 49. A. M. Kloosterman, K. E. Shelton, G. P. van Wezel, M. H. Medema, D. A. Mitchell,
771 RRE-Finder: a Genome-Mining Tool for Class-Independent RiPP Discovery.
772 *mSystems* **5**, e00267-00220 (2020).
773 50. J. Söding, A. Biegert, A. N. Lupas, The HHpred interactive server for protein
774 homology detection and structure prediction. *Nucleic Acids Res* **33**, W244-248
775 (2005).
776 51. D. T. Jones, Protein secondary structure prediction based on position-specific scoring
777 matrices. *Journal of Molecular Biology* **292**, 195-202 (1999).
778 52. T. Petnicki-Ocwieja *et al.*, Genomewide identification of proteins secreted by the Hrp
779 type III protein secretion system of *Pseudomonas syringae* pv. *tomato* DC3000. *Proc*
780 *Natl Acad Sci U S A* **99**, 7652-7657 (2002).
781
782

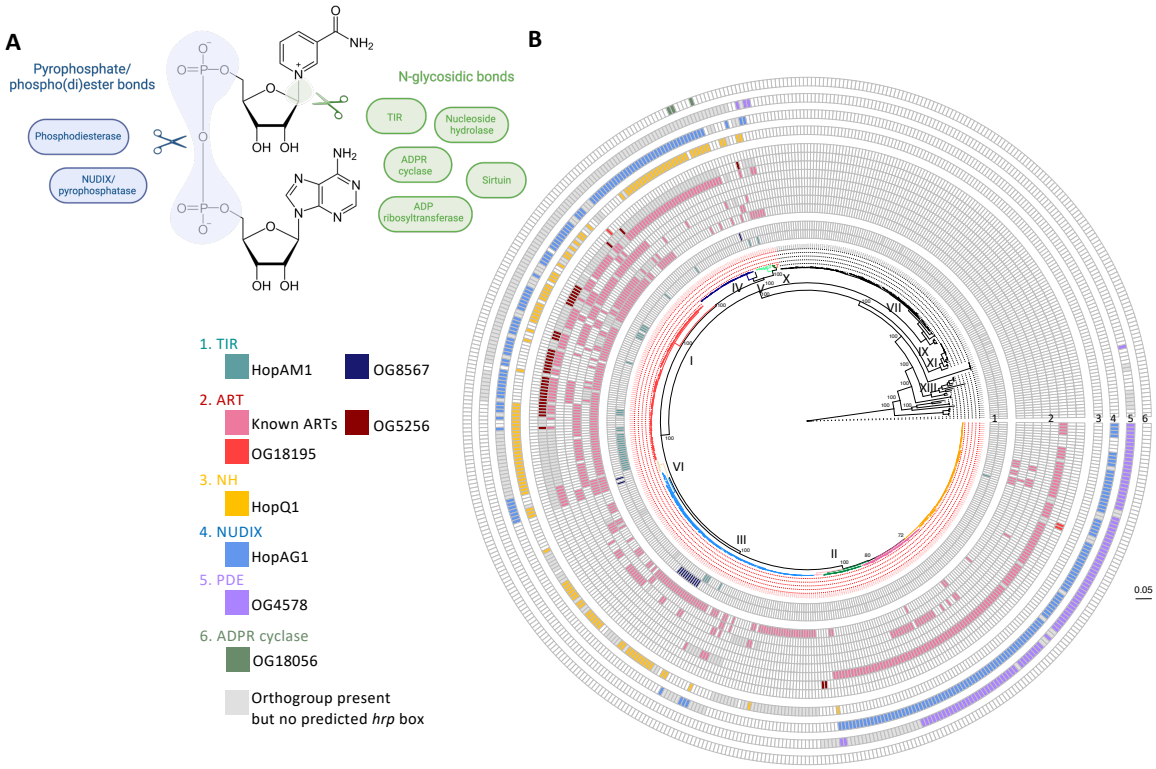
A
Pyrophosphate/
phospho(di)ester bonds
Phosphodiesterase
NUDIX/
pyrophosphatase
N-glycosidic bonds
TIR
Nucleoside
hydrolase
ADPR
cyclase
Sirtuin
ADP
ribosyltransferase
1. TIR
HopAM1
OG8567
2. ART
Known ARTs
OG5256
OG18195
3. NH
HopQ1
4. NUDIX
HopAG1
5. PDE
OG4578
6. ADPR cyclase
OG18056
Orthogroup present
but no predicted hrp box
B
0.05

783

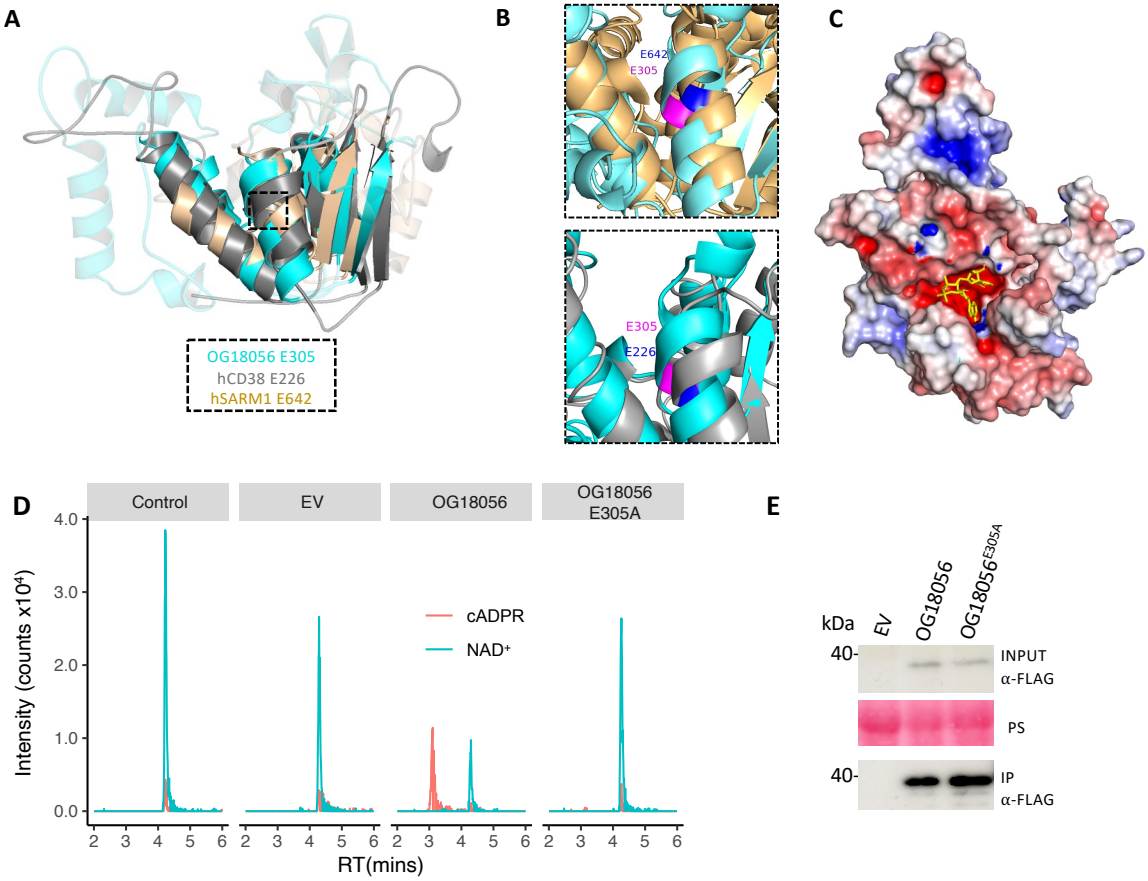
A
OG18056 E305
hCD38 E226
hSARM1 E642
B
E642
E305
E305
E226
C
D
Control
EV
OG18056
OG18056 E305A
Intensity (counts x10⁴)
4.0
3.0
2.0
1.0
0.0
cADPR
NAD+
RT(mins)
E
kDa
EV
OG18056
OG18056E305A
40-
INPUT
α-FLAG
PS
40-
IP
α-FLAG

784

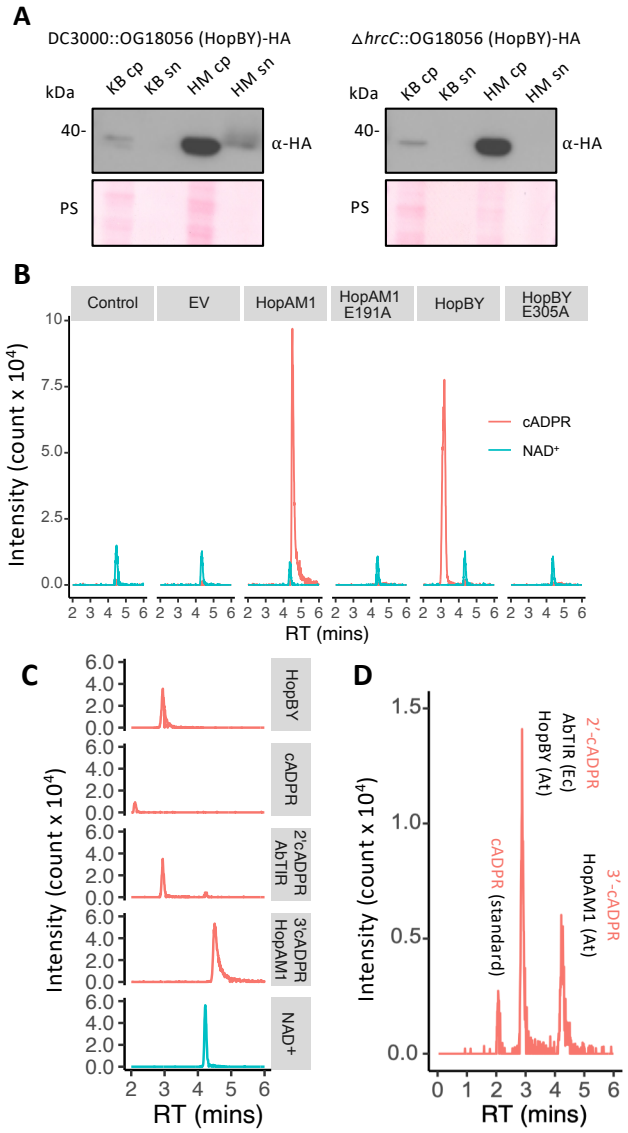
A
DC3000::OG18056 (HopBY)-HA
ΔhrcC::OG18056 (HopBY)-HA
kDa
KB cp
KB sn
HM cp
HM sn
40-
α-HA
PS
B
Control
EV
HopAM1
HopAM1 E191A
HopBY
HopBY E305A
Intensity (count x 10⁴)
cADPR
NAD+
RT (mins)
C
HopBY
cADPR
2'cADPR AbTIR
3'cADPR HopAM1
NAD+
D
cADPR (standard)
HopBY (At)
AbTIR (Ec)
2'-cADPR
HopAM1 (At)
3'-cADPR

785

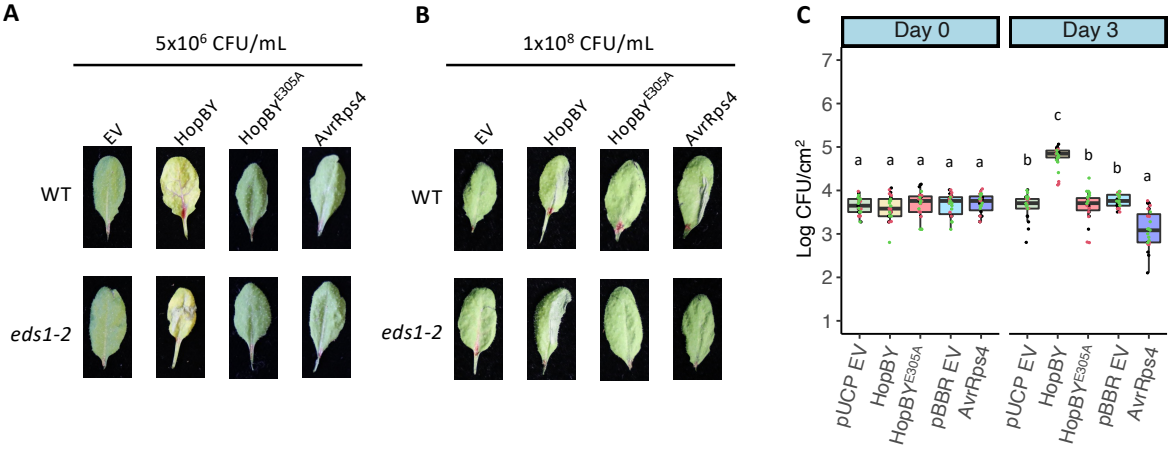
A
5x10⁶ CFU/mL
EV
HopBY
HopBY^E305A
AvrRps4
WT
eds1-2
B
1x10⁸ CFU/mL
EV
HopBY
HopBY^E305A
AvrRps4
WT
eds1-2
C
Day 0
Day 3
Log CFU/cm²
7
6
5
4
3
2
1
a a a a a
b c b b a
pUCP EV
HopBY
HopBY^E305A
pBBR EV
AvrRps4
pUCP EV
HopBY
HopBY^E305A
pBBR EV
AvrRps4

786

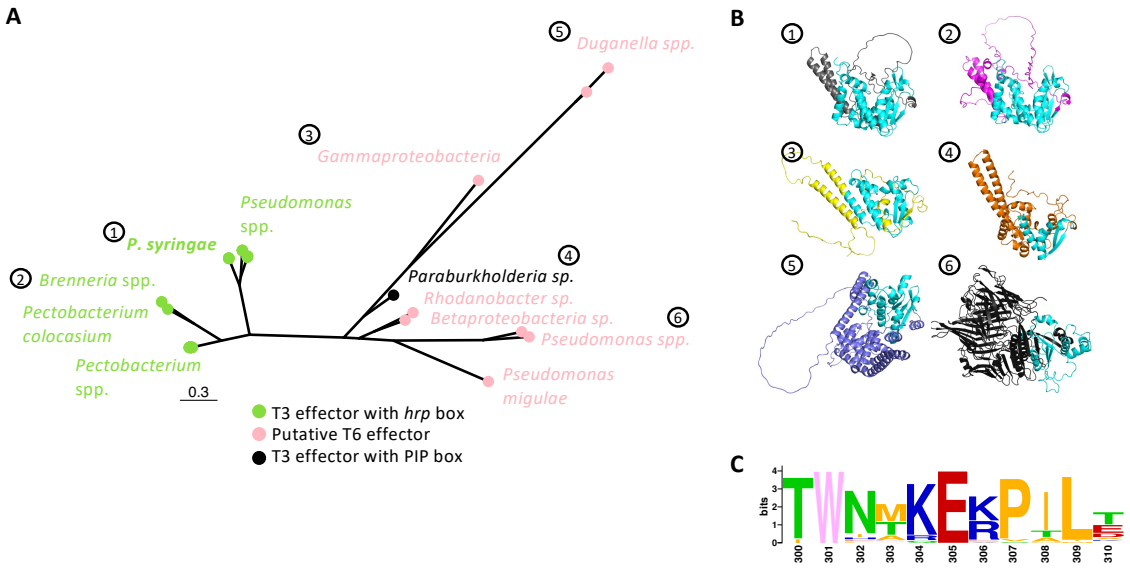
A
B
C
Duganella spp.
Gammaproteobacteria
Pseudomonas spp.
P. syringae
Brenneria spp.
Pectobacterium colocasium
Pectobacterium spp.
Paraburkholderia sp.
Rhodanobacter sp.
Betaproteobacteria sp.
Pseudomonas spp.
Pseudomonas migulae
0.3
T3 effector with hrp box
Putative T6 effector
T3 effector with PIP box
bits
300
301
302
303
304
305
306
307
308
309
310

787